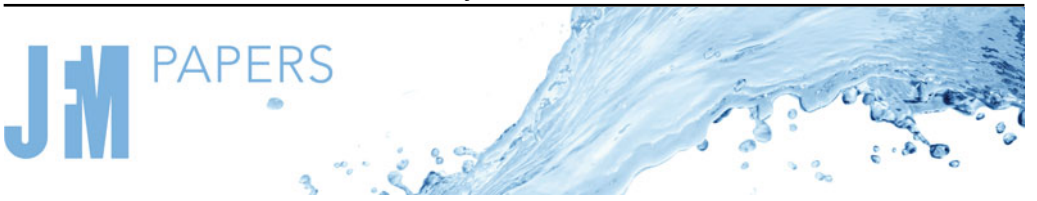
J. Fluid Mech. (2026), *vol.* 1026, A51, doi:10.1017/jfm.2025.11071



Localised inter-scale energy cascades in free-surface turbulence

Guotao Wu[1], **Yaxing Li**[1] **and Filippo Coletti**[2]

[1]Department of Engineering Mechanics, School of Aeronautics and Astronautics, Zhejiang University, Hangzhou 310027, PR China

[2]Department of Mechanical and Process Engineering, ETH Zürich, Zürich 8092, Switzerland

Corresponding author: Yaxing Li, yaxingli@zju.edu.cn

(Received 9 July 2025; revised 1 November 2025; accepted 12 December 2025)

The energy of fluid turbulence is transported, on average, to smaller and larger scales in three-dimensional and two-dimensional flows, respectively. The motion along the flat free surface of a turbulent liquid shares similarities with both classes of flows, therefore the direction of the energy cascade along it is ambiguous. We show experimentally that the process is linked to the local divergence of the surface velocity field: expansive motions, associated with flow upwelling towards the surface, transfer energy to larger scales, while compressive motions, associated with fluid plunging into the bulk, do the opposite. The net inter-scale energy flux is therefore vanishingly small, in stark contrast with homogeneous turbulence in both two- and three-dimensional systems. Moreover, we find that rare and intense compressive/expansive events are chiefly responsible for the instantaneous inter-scale fluxes, which are much stronger than their counterparts at depth.

Key words: waves/free-surface flows, homogeneous turbulence, multiphase flow

1. Introduction

Turbulent flows below and along free surfaces are ubiquitous, encompassing all natural water bodies and countless industrial processes. The associated dynamics are vital on a global scale, affecting enthalpy flux, gas exchange and aerosol production at the air–water interface of oceans, rivers and lakes (Jähne & Haussecker 1998; Deike 2022), as well as the dispersion of floating micro- and macro-plastics (van Emmerik & Schwarz 2020; van Sebille *et al.* 2020). When the surface undergoes significant deformations, the behaviour is complicated by gravity-capillary waves (Brocchini & Peregrine 2001; Smeltzer *et al.* 2023). Even when the interface is approximately flat, the situation remains deceptively intricate (Magnaudet 2003). As remarked in early studies by Goldburg *et al.*

© The Author(s), 2026. Published by Cambridge University Press.

https://doi.org/10.1017/jfm.2025.11071 Published online by Cambridge University Press

(2001) and Eckhardt & Schumacher (2001), the surface flow has several specific features. Although the liquid motion is divergence-free, the velocity field along the free surface is compressible, which leads to intense clustering of floating particles (Schumacher & Eckhardt 2002; Boffetta *et al.* 2004; Cressman *et al.* 2004) and affects relative dispersion (Li *et al.* 2024). Moreover, as the surface exchanges energy and enstrophy with the underlying fluid, scaling arguments for the flux and scale-to-scale distribution of such quantities are missing (Goldburg *et al.* 2001). While this is true of any two-dimensional (2-D) section exchanging energy and enstrophy with the three-dimensional (3-D) domain from which it is extracted, the surface flow is peculiar in that fluid elements on the surface remain confined on it (as the vertical velocity vanishes). This makes it especially relevant to characterise the dynamics defined by the surface velocity field, as this fully determines the Lagrangian transport. We remark that although energy and enstrophy are not conserved, the flow may still be characterised by significant scale-to-scale fluxes of such quantities locally in space/time. Even in cases when a net cascade is established, as in 3-D homogeneous isotropic turbulence (HIT), the local fluxes of energy to both smaller and larger scales can be very large (Yasuda & Vassilicos 2018; Yao *et al.* 2024*b*).

Previous experimental and numerical studies indicated that in the considered limit of negligible surface deformation, the motion of the fluid element along the surface possesses features associated with both 3-D and 2-D turbulence. On one hand, free-surface flows display intermittent accelerations and velocity gradients typical of 3-D turbulence, and in fact to a higher degree (Eckhardt & Schumacher 2001; Goldburg *et al.* 2001; Qi, Li & Coletti 2025*b*). On the other hand, long-lived vortices are prevalent, reminiscent of 2-D turbulence (Pan & Banerjee 1995; Kumar, Gupta & Banerjee 1998; Sanness Salmon *et al.* 2023; Li *et al.* 2025; Qi *et al.* 2025*a*). This duality naturally raises the question: how is the energy associated with free-surface turbulent motion transported across scales? It is indeed well known that the inter-scale energy transfer differs fundamentally between 3-D and 2-D turbulence, manifesting as direct (downscale) and inverse (upscale) energy cascades, respectively (Alexakis & Biferale 2018).

In previous numerical studies, the answer was found to depend on the specific flow configurations. Lovecchio, Zonta & Soldati (2015) associated the upscale and downscale energy transfer at the free surface with the 2-D divergence of the surface velocity in open channel flow. They pointed out how, even though driven by the underlying 3-D turbulence, the surface flow is characterised by an upscale energy transfer that controls the long-term evolution of the large scales. The recent numerical investigation by Boffetta *et al.* (2023), however, indicated that turbulence in the vicinity of a free surface exhibits a transient inverse energy cascade, particularly in relatively thin fluid layers, before transitioning to a 3-D direct cascade. Most of these studies imposed a strictly flat surface that affects the inter-component energy transfer and did not achieve sufficient scale separation to establish an inertial subrange (Shen *et al.* 1999; Guo & Shen 2010). Experimental studies have focused on the vertical transport of energy between the turbulent bulk and the near-surface region, suggesting a blend of direct and inverse cascade depending on the spatial directions and velocity components (Ruth & Coletti 2024). Overall, the magnitude and underlying mechanism of inter-scale energy transfers in the fundamental case of a flat free surface above homogeneous turbulence are not fully understood.

In this study, we seek a mechanistic understanding of the inter-scale energy transfer associated with the turbulence along and adjacent to the free surface. We consider the case in which an approximately flat surface bounds a region of otherwise homogeneous turbulence. The energy distribution in the space of separations $\boldsymbol{r}$ is described by the second-order velocity structure function $\overline{(\delta \boldsymbol{u})^2}$, where $\delta \boldsymbol{u}$ is the velocity increment

https://doi.org/10.1017/jfm.2025.11071 Published online by Cambridge University Press

between points separated by $\boldsymbol{r}$, and the overbar indicates ensemble-averaging (in time and along homogeneous spatial directions). The energy transport across scales is classically evaluated by considering the nonlinear inter-scale energy transfer rate Π, that is, the divergence in scale space of the nonlinear inter-scale flux density vector $\overline{\delta\boldsymbol{u}\,(\delta\boldsymbol{u})^2}$. In the inertial range of stationary 3-D HIT, one retrieves the celebrated Kolmogorov's 4/5 law, classically expressed in terms of the third-order longitudinal structure function $\overline{\delta u_L^3} = -4/5\epsilon r$, where $\delta u_L = \delta\boldsymbol{u}\cdot\boldsymbol{r}/r$ (Kolmogorov 1941), and the equilibrium relation $\Pi = -\epsilon$, ϵ being the dissipation rate of the turbulent kinetic energy (see Vassilicos (2015) for a review). In general flow configurations in which temporal steady state and/or spatial homogeneity are not realised, the inter-scale energy flux is also balanced by transfers in physical space and time, according to the Kármán–Howarth–Monin–Hill (KHMH) equation, also referred to as the generalised Kolmogorov equation (Hill 2002). This framework has been extensively used to investigate non-homogeneous/non-isotropic flows, e.g. wall-bounded turbulence (Marati, Casciola & Piva 2004; Cimarelli *et al.* 2013, 2024), rotating turbulence (Lamriben, Cortet & Moisy 2011), decaying grid turbulence (Valente & Vassilicos 2015), jets (Cimarelli *et al.* 2021), wakes (Gomes-Fernandes, Ganapathisubramani & Vassilicos 2015; Vassilicos 2015; Portela, Papadakis & Vassilicos 2017), and recently in free-surface turbulence (Ruth & Coletti 2024). The same framework has also provided insight into steady homogeneous turbulence, revealing the magnitude and mutual correlations between the instantaneous/local transfers in scale space and physical space (Carter & Coletti 2018; Yasuda & Vassilicos 2018; Yao *et al.* 2024*a*).

Here, we focus on how the energy along the surface located at $z = 0$ (where z is the vertical upward axis) is transferred across scales, thus restricting our attention to separations and velocities along surface-parallel $x-y$ planes. The kinematic boundary condition $u_z = 0$ implies that in the limit of vanishing surface deformations, those components capture the entire energy of the surface flow. In the spirit of the KHMH equation, given two points $\boldsymbol{X}$ and $\boldsymbol{X}'$ separated by $\boldsymbol{r} = \boldsymbol{e}_x r_x + \boldsymbol{e}_y r_y$ and associated with velocity fluctuations $\boldsymbol{u}$ and $\boldsymbol{u}'$, one considers the increment $\delta\boldsymbol{u}(\boldsymbol{r}) = \boldsymbol{u} - \boldsymbol{u}'$ and the associated energy $\delta q^2 = (\delta\boldsymbol{u})^2 = \delta u_x^2 + \delta u_y^2$. The orientation of the energy flux $\overline{\delta\boldsymbol{u}\,\delta q^2}$ characterises the direction where energy flows in scale space, directly linking to the concept of energy cascade. With the assumption of local isotropy, the flux only has a radial component pointing from large to small separations for any orientation, leading to the Richardson–Kolmogorov equilibrium cascade in HIT. In the absence of isotropy, the orientation of $\overline{\delta\boldsymbol{u}\,\delta q^2}$ varies with the orientation of the separation vector $\boldsymbol{r}$, implying that δq^2 is also redistributed in scale space, rather than solely transferred across scales (Portela *et al.* 2017). Hence in our 2-D surface system, the evaluation of the direction of energy cascade requires the radial components of the energy flux. In polar coordinates, it is expressed as (Gomes-Fernandes *et al.* 2015) $S_r = \overline{\delta u_r\,\delta q^2}$, where $\delta u_r = \delta\boldsymbol{u}\cdot\boldsymbol{r}/r$. For $S_r < 0$, the energy is transferred from large to small scale; conversely, for $S_r > 0$, the energy flux is from small to large scale. As discussed by Portela *et al.* (2017) among others, the sign of S_r is not sufficient to characterise the energy cascade as being direct or inverse. For the energy cascade across scales to be direct over a given range of separations, S_r and the radial component of the nonlinear inter-scale transfer rate $\Pi_r = 1/(4r^2)\,\partial(r^2\,\overline{\delta u_r\,\delta q^2})/\partial r$ should both be negative; whereas both should be positive for the cascade to be characterised as inverse.

In this work, we conduct experimental measurements of the 2-D velocity field in the vicinity of the quasi-flat free surface above steady forced turbulence, aiming to

https://doi.org/10.1017/jfm.2025.11071 Published online by Cambridge University Press

Re_λ	u'_x (cm s^{-1})	u'_y (cm s^{-1})	ϵ (m^2 s^{-3})	η (mm)	τ_η (s)	$\mathcal{L}$ (cm)
326	5.08	3.33	3.6×10^{-4}	0.23	0.05	9.1

Table 1. Main turbulence statistics for the homogeneous turbulence evaluated in the bulk, i.e. more than one integral scale below the surface. Here, Re_λ is the Taylor-scale Reynolds number, u'_x and u'_y are the r.m.s. velocities parallel and perpendicular to the jet direction, respectively, ϵ is the dissipation rate, η, τ_η are the Kolmogorov length and time scale, respectively, and $\mathcal{L}$ is the integral length scale calculated from weighted averages between directions x and y (Carter & Coletti 2017).

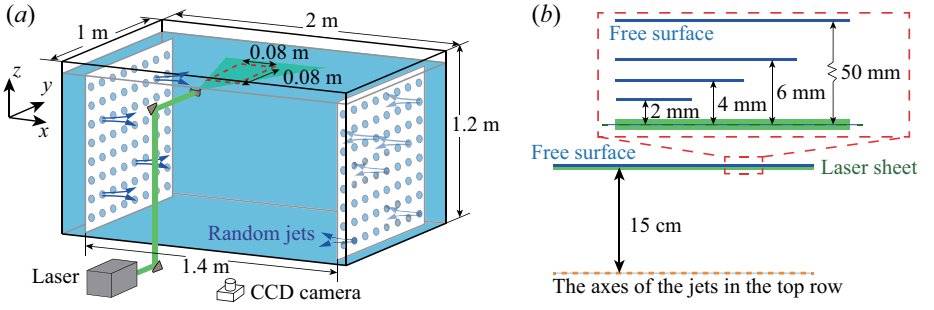


Figure 1. (*a*) Schematic of the experimental set-up. (*b*) Illustration of the PIV settings. The 1.5 mm thick laser sheet is horizontally directed underneath the free surface.

quantitatively investigate the inter-scale energy cascade by the nonlinear interactions. The rest of the paper is organised as follows. In § 2, we describe the experimental methodology and evaluate the flow properties in our set-up. Then we analyse the experimental data in § 3. Section 4 summarises our findings and draws conclusions.

2. Methods

2.1. *Experimental method*

We conducted planar particle image velocimetry (PIV) measurements along surface-parallel planes in the near-surface region of a large zero-mean-flow turbulent water tank. The experimental apparatus was described in detail elsewhere (Li *et al.* 2024; Ruth & Coletti 2024; Qi *et al.* 2025*a*,*b*) and is illustrated in figure 1. It features two facing arrays of zero-mean-flow pumps, firing turbulent jets in randomised sequence inside a 2 m^3 volume. The power of the pumps is modulated to obtain the turbulence properties listed in table 1 in the homogeneous central region, below the layer influenced by the surface ($z < -\mathcal{L}$, where $\mathcal{L}$ is the integral length scale of the turbulence; Hunt & Graham 1978; Magnaudet 2003). This set-up achieves higher turbulent Reynolds number Re_λ compared to previous studies, establishing a well-developed inertial subrange (Ruth & Coletti 2024). The distance between the surface and the top row of firing jets varies between 15 and 20 cm. This configuration is comparable to previous experiments (Brumley & Jirka 1987; McKenna & McGillis 2004; Herlina & Jirka 2008; Variano & Cowen 2008, 2013) and simulations (Guo & Shen 2010; Herlina & Wissink 2014) in which the turbulence decays spatially towards the surface from the forcing region at depth. We verify that the surface displays only sub-millimetre deformations. To investigate the influence of the surface, the distance between the latter and the measurement plane is varied between 2 and 50 mm. The uppermost plane is at the edge of the viscous layer in which the vertical velocity

https://doi.org/10.1017/jfm.2025.11071 Published online by Cambridge University Press

z (mm)	u'_x (cm s^{-1})	u'_y (cm s^{-1})	IF	HD	$MSRF$	$\overline{C}$
−2	3.48	3.18	0.94	0.032	0.041	0.45
−4	3.48	3.08	0.96	0.037	0.043	0.43
−6	3.30	2.83	0.97	0.029	0.039	0.30
−50	2.59	2.09	0.98	0.039	0.034	0.24

Table 2. Main sub-surface turbulence statistics for the case $Re_\lambda = 326$. Here, z is the distance between the turbulence free surface and the PIV measurement plane, and u'_x and u'_y are the r.m.s. velocities parallel and perpendicular to the jetting direction, respectively. The compressibility coefficient $\overline{C}$, the small-scale isotropy factor IF, the homogeneity deviation HD and the mean strain-rate factor $MSRF$ are defined in the text.

gradients vanish, to satisfy the zero-shear-stress condition at the surface (Ruth & Coletti 2024). Therefore, the measurements are expected to capture the dynamics of the surface flow.

For each measurement, 3000 image pairs are recorded at sample rate 1 Hz using a CCD camera (Imperx 6600 × 4400 pixels, 5.5 μm pixel size) coupled with a 200 mm lens (Nikon, $f = 5.6$). A double-pulse laser sheet with 1.5 mm thickness is directed horizontally by an Nd:YAG laser (Beamtech, 532 nm wavelength, 500 mJ pulse^{-1}) to illuminate 10 μm hollow glass sphere tracer particles. Velocity vectors are calculated using an iterative cross-correlation algorithm with window offset and deformation. The first 128 × 128 pixel pass is refined to 64 × 64 pixel with a 50 % overlap, leading to vector spacing 0.635 mm. A Gaussian fitting function is used to determine subpixel displacements.

To limit the accumulation of surfactants and other contamination, the water surface was periodically skimmed and vacuumed before every measurement: a water vacuum is positioned close to the water surface, aspirating a thin layer of the surface water, along with any accumulated contaminants. Though some contamination is unavoidable, the surface tension of the working fluid, measured via a contact angle measuring instrument at various points in time, remained at the standard value 0.07 N m^{-1} during the experiments.

2.2. *Flow properties*

As the surface is approached, the vertical component of the normal Reynolds stresses is redirected in the surface-parallel direction (Hunt & Graham 1978), as signalled by the increasing fluctuations measured along PIV planes (table 2). The measured instantaneous velocity is Reynolds decomposed into the local mean velocity U_i and the local velocity fluctuations u_i, the former being negligibly small (Li *et al.* 2024; Ruth & Coletti 2024). The root mean square of the velocity fluctuations (r.m.s. velocity) is defined as $u'_i = \sqrt{\overline{u_i^2}}$. To evaluate to which degree the surface flow approximates homogeneous and isotropic conditions, we follow Carter *et al.* (2016) and compute the small-scale isotropic factor $IF = \overline{|(\partial u_x/\partial x)/(\partial u_y/\partial y)|}$, the homogeneity deviation $HD = 2\sigma_u/u'$ (where σ_u is the spatial standard deviation of the local ensemble average of the velocity fluctuations $\sqrt{\overline{u_i^2}}$), and the mean strain-rate factor $MSRF = \left\langle \sqrt{(\partial U_x/\partial x)^2 + (\partial U_y/\partial y)^2} \right\rangle / \overline{\sqrt{\langle (\partial u_x/\partial x)^2 + (\partial u_y/\partial y)^2 \rangle}}$. Here, $\langle\cdot\rangle$ denotes spatial averaging. The values of IF, HD and $MSRF$ indicate approximate small-scale isotropy, high spatial homogeneity and negligible mean velocity gradients along the $x-y$ plane.

https://doi.org/10.1017/jfm.2025.11071 Published online by Cambridge University Press

To describe the topology of the surface velocity field, we consider the reduced velocity gradient tensor $\tilde{\boldsymbol{A}}$, i.e. the upper 2×2 block of the full velocity gradient tensor $A_{ij} = \partial u_i/\partial x_j$, defined by in-plane gradients of the surface-parallel velocity components (Cardesa *et al.* 2013; Qi *et al.* 2025*b*). One of the key features of free-surface turbulence is the exchange of mass and energy with the bulk, through upwelling and downwelling structures that carry fluid towards and from the surface, respectively (Pan & Banerjee 1995). The kinematic boundary condition implies that the surface divergence $\mathcal{D} = \tilde{A}_{ii}$ is positive above upwellings and negative above downwellings. These regions of expansion and compression reflect the non-solenoidal nature of free-surface flows, quantified by the compressibility coefficient $\overline{\mathcal{C}} = \overline{\tilde{A}_{ii}^2}/\overline{\tilde{A}_{ij}^2}$ (Eckhardt & Schumacher 2001; Goldburg *et al.* 2001; Cressman *et al.* 2004). The level of compressibility has far-reaching consequences for the relative motion (Csanady 1963; Li *et al.* 2024) and spatial distribution of floating particles (Boffetta *et al.* 2004; Lovecchio, Marchioli & Soldati 2013; Li *et al.* 2025). As we will show, it is crucial for the inter-scale energy transfer, too. Approaching the surface, the compressibility coefficient (which in the bulk is comparable to the theoretical value $\overline{\mathcal{C}} = 1/6$ expected for a 2-D cut through 3-D HIT; Boffetta *et al.* 2004) approaches the condition $\overline{\mathcal{C}} = 0.5$, implying that the in-plane longitudinal velocity gradients are uncorrelated, $\overline{(\partial u_x/\partial x)(\partial u_y/\partial y)} \approx 0$ (Eckhardt & Schumacher 2001; Goldburg *et al.* 2001; Cressman *et al.* 2004; Li *et al.* 2025).

3. Results

3.1. *Compressibility of surface flow*

To characterise the flow topology of the compressible surface flow, we consider the joint probability distribution function (p.d.f.) of the two invariants of the reduced velocity gradient tensor $\tilde{A}$, $p = -\tilde{A}_{ii}$ and $q = -\det(\tilde{A})$, respectively (Perry & Chong 1994). The former characterises the divergence of the surface flow, while the latter captures the combined instantaneous stretching and rotation rates along the two principal directions. As shown in figures 2(*a*1–*a*4), the joint p.d.f.s exhibit a characteristic teapot shape typical of 2-D sections across 3-D turbulent flows (Cardesa *et al.* 2013; Carter & Coletti 2018). Notably, the probability distribution of p displays heavier tails as the free surface is approached, indicating increased probability of intense expanding and contracting pattern (Qi *et al.* 2025*b*), consistent with the observation that $\overline{\mathcal{C}}$ grows approaching the surface. The red dashed line in each image marks $q = p^2/4$, i.e. the boundary across which the local flow topology changes between stable/unstable foci and stable/unstable nodes. This indicates the transition between focus-type (rotation-dominated) and node-type (strain-dominated) regions in the phase portrait (Perry & Chong 1994). Note that the p–q joint p.d.f. of the 2-D surface velocity field shows a pattern differing significantly from the one measured in 2-D sections of 3-D turbulence in the bulk of the water tank. The latter is reported in figure 7 in Appendix A, and matches the pattern expected in homogeneous regions of 3-D turbulence (Cardesa *et al.* 2013).

Figure 2(*b*) plots the p.d.f.s of instantaneous spatially averaged compressibility coefficient $\langle \mathcal{C} \rangle = \langle \tilde{A}_{ii}^2 \rangle / \langle \tilde{A}_{ij}^2 \rangle$. It is shown that the peak of the p.d.f. moves towards higher value of $\langle \mathcal{C} \rangle$, and the distribution also becomes more spread out. Near the surface, figures 2(*c*1,*c*2) illustrate two instantaneous fields of normalised near-surface divergence $\mathcal{D}\tau_\eta$ (where τ_η is the Kolmogorov time scale) associated with different instantaneous values of $\langle \mathcal{C} \rangle$. When the latter is large, strongly divergent and convergent flow regions are visible.

https://doi.org/10.1017/jfm.2025.11071 Published online by Cambridge University Press

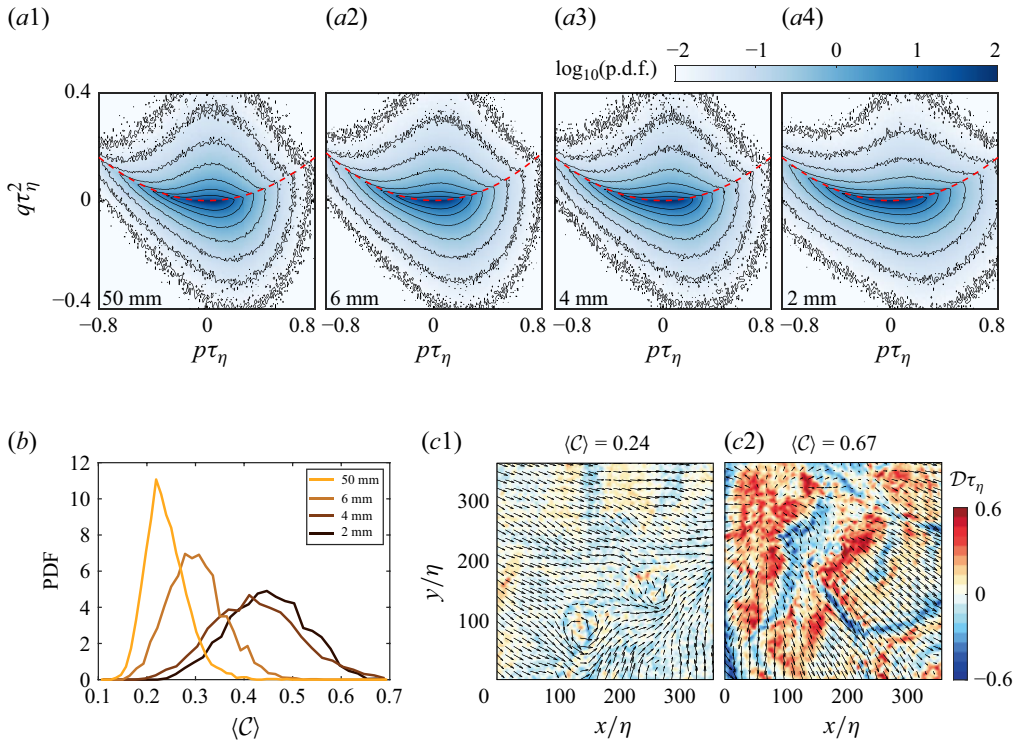


Figure 2. (*a*) The joint p.d.f.s of normalised p and q at $Re_\lambda = 326$ along the 2-D PIV plane for all the considered cases at different distances from the free surface: (*a*1) 50 mm, (*a*2) 6 mm, (*a*3) 4 mm, (*a*4) 2 mm. The logarithmic contours range from 10^{-2} to 10^{1}, with adjacent contours being separated by half a decade. In all four panels, the red dashed lines mark $q = p^2/4$. (*b*) The p.d.f.s of instantaneous spatially averaged compressibility coefficient $\langle\mathcal{C}\rangle = \langle\tilde{A}_{ii}^2\rangle/\langle\tilde{A}_{ij}^2\rangle$. (*c*) Instantaneous divergence and velocity field on the free surface with instantaneous compressibility coefficients (*c*1) $\langle\mathcal{C}\rangle = 0.24$ and (*c*2) $\langle\mathcal{C}\rangle = 0.67$. The colour map represents the local divergence $\mathcal{D}$ normalised by the Kolmogorov time scale τ_η, and the arrows indicate the velocity vector $\boldsymbol{u}$.

3.2. *Inter-scale energy transfer and flow structure*

Focusing on this near-surface plane, we then analyse the inter-scale energy transfer conditioned on the spatially averaged divergence $\langle\mathcal{D}\rangle$. The probability distribution of $\langle\mathcal{D}\rangle\tau_\eta$ is nearly a Gaussian with nearly zero mean and standard deviation $\sigma_{\langle\mathcal{D}\rangle} \approx 0.027$. Via the nominal threshold $\pm 1.5\sigma_{\langle\mathcal{D}\rangle} \approx \pm 0.04$, we define four flow states based on the magnitude and sign of the divergence: $\langle\mathcal{D}\rangle\tau_\eta < -0.04$, $\langle\mathcal{D}\rangle\tau_\eta \in [-0.04, 0]$, $\langle\mathcal{D}\rangle\tau_\eta \in [0, 0.04]$ and $\langle\mathcal{D}\rangle\tau_\eta > 0.04$. (Somewhat different values of the threshold do not alter the outcome of the following analysis.) With this definition, the probability of the occurrence of strong-divergence states ($|\langle\mathcal{D}\rangle|\,\tau_\eta > 0.04$) is approximately 13 %. As the flow is approximately homogeneous and isotropic along the measurement plane, we use polar coordinates and focus on the radial component of the nonlinear inter-scale energy transfer rate Π_r and the energy flux density S_r, which are responsible for the transport across scales as discussed in § 1. Figures 3(*a*1) and 3(*b*1) display scale-dependent plots of S_r and Π_r, respectively, conditioned on the four above-mentioned states. The existence of a direct energy cascade requires both S_r and Π_r to be negative, whereas the two should be positive for the cascade to be inverse (Portela *et al.* 2017). In the present case, when the divergence is strongly positive ($\langle\mathcal{D}\rangle\tau_\eta > 0.04$), an intense inverse energy cascade is realised, and vice

https://doi.org/10.1017/jfm.2025.11071 Published online by Cambridge University Press

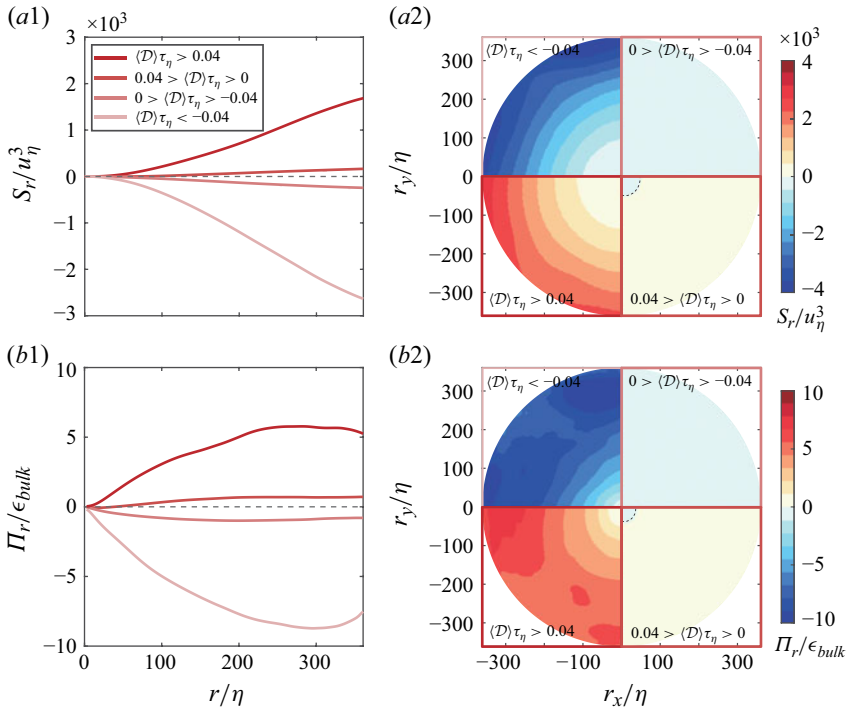


Figure 3. Energy flux density and the nonlinear energy transfer rate measured in the 2-D plane 2 mm away from the free surface. (*a*1,*a*2) Radial component of the flux of S_r normalised by u_η^3 for four ranges of spatial-averaged divergence. (*b*1,*b*2) Radial component of the nonlinear scale-to-scale energy transfer Π_r normalised by the dissipation rate in the bulk ϵ_{bulk}.

versa when it is strongly negative: as $\langle\mathcal{D}\rangle$ shifts from negative to positive, the direction of the inter-scale energy transfer changes. The magnitudes of S_r and Π_r in weak-divergence states ($|\langle\mathcal{D}\rangle|\,\tau_\eta < 0.04$) are significantly smaller than those in strong-divergence states, although the latter occur much less frequently. This indicates that intense and relatively rare compressive/expansive motions are the main drivers of the energy cascade at the free surface. Remarkably, normalisation by the turbulent dissipation in the bulk, ϵ_{bulk}, reveals that the inter-scale fluxes in strong-divergence states are much higher than away from the surface, where on average $\Pi_r \approx \epsilon_{bulk}$. The polar diagrams in figures 3(*a*2) and 3(*b*2) confirm that despite the large-scale anisotropy due to the directional forcing, the process is approximately isotropic, the radial fluxes being approximately independent on the direction of separation along the surface.

While the above analysis is purely statistical, one may expect a correlation between inter-scale energy transfers and local flow structures. To verify this picture, we define highly expansive/compressive structures as contiguous regions satisfying the condition $|\mathcal{D}| > \alpha_\mathcal{D}\sqrt{\overline{\mathcal{D}^2}}$, where $\alpha_\mathcal{D}$ is a positive constant. To determine the appropriate value of the constant, we analyse the percolation behaviour of such high-intensity regions. Borrowing approaches employed to identify turbulent coherent structures (Moisy & Jiménez 2004; Carter & Coletti 2018), we consider how the number and size of the structures changes as the threshold is varied. Figures 4(*a*1–*a*4) display a normalised instantaneous divergence $\mathcal{D}$ field with the resulting expansive/compressive structures identified by a range of threshold levels. Figure 4(*b*) indicates that both the number and size of the structures are maximised for $\alpha_\mathcal{D} \approx 0.8$. Based on the latter, highly expansive/compressive regions

https://doi.org/10.1017/jfm.2025.11071 Published online by Cambridge University Press

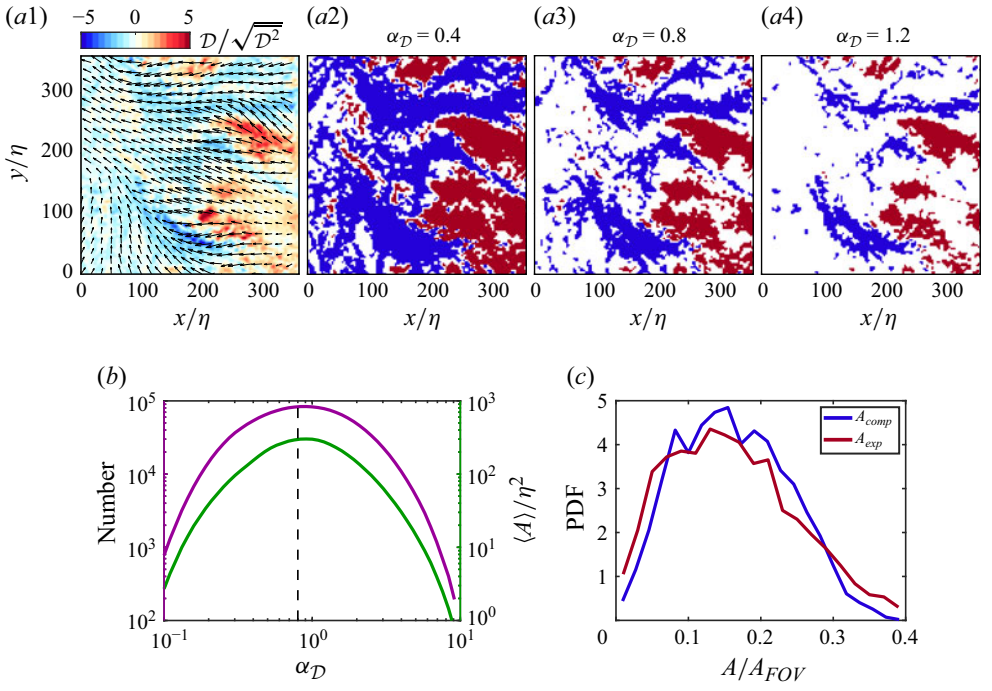


Figure 4. (*a*1) Normalised instantaneous divergence $\mathcal{D}$ field for the measurement in the 2-D plane 2 mm away from the free surface, with resulting expansive/compressive structures identified by thresholds (*a*2) $\alpha_{\mathcal{D}} = 0.4$, (*a*3) $\alpha_{\mathcal{D}} = 0.8$ and (*a*4) $\alpha_{\mathcal{D}} = 1.2$. (*b*) Percolation diagram with the total number (purple) and the mean area (green) of high-intensity structures found in the FOV as a function of thresholds $|\mathcal{D}| > \alpha_{\mathcal{D}}\sqrt{\overline{\mathcal{D}^2}}$. (*c*) The p.d.f. of the portion of area in the FOV for compressive (blue) and expansive (red) structures.

are defined. The broad range of sizes can be appreciated, which results in a power-law size distribution (Qi *et al.* 2025*a*). The p.d.f.s of the fractional area occupied by highly expansive (A_{exp}) and highly compressive (A_{comp}) structures in the field of view (FOV) (of area A_{FOV}) are similar (figure 4*c*), implying that both types of events occur with comparable frequency.

We partition the ensemble of near-surface flow fields in strong-divergence state ($(A_{exp} + A_{comp})/A_{FOV} > 1/2$) based on the sign of $A_{exp} - A_{comp}$. The conditional behaviour of S_r and Π_r confirms that realisations in which compression (hence downwellings) prevail are characterised by a direct energy cascade from large to small scales, and vice versa; see figure 5. In both situations, the magnitude of Π_r in the inertial subrange is much greater than in the bulk. This demonstrates that upwellings/expansions and downwellings/compressions are highly effective at transferring energy to larger and smaller scales, respectively. In the framework of the KHMH equation, those structures balance the surface-normal energy fluxes (associated with transport in physical space) with surface-parallel fluxes (in scale space). Because both upwellings and downwellings are characterised by similar intensity and frequency of occurrence, the net inter-scale transfer within the surface flow is marginal. We note that while continuity imposes that the global mass transfers to and from the surface cancel out, some systematic asymmetry in the kinematics of upwellings and downwellings was reported (Guo & Shen 2010; Ruth & Coletti 2024), leaving the possibility of a non-zero (albeit weak) net cascade.

In order to further link the nonlinear energy flux with the local flow structure, we implement the filter-space technique to compute the scale-to-scale energy transfer flux Π^{Δ}

https://doi.org/10.1017/jfm.2025.11071 Published online by Cambridge University Press

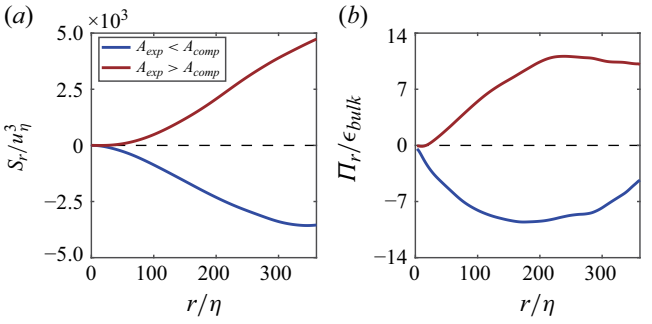


Figure 5. Energy flux density and the nonlinear energy transfer rate measured in the 2-D plane 2 mm away from the free surface. (*a*) Radial component of the flux density S_r normalised by u_η^3 for two states. (*b*) Radial component of the nonlinear scale-to-scale energy transfer Π_r normalised by the dissipation rate in the bulk ϵ_{bulk}. All the calculations are conditioned by the relation between the total area of source A_{exp} and sink A_{comp}.

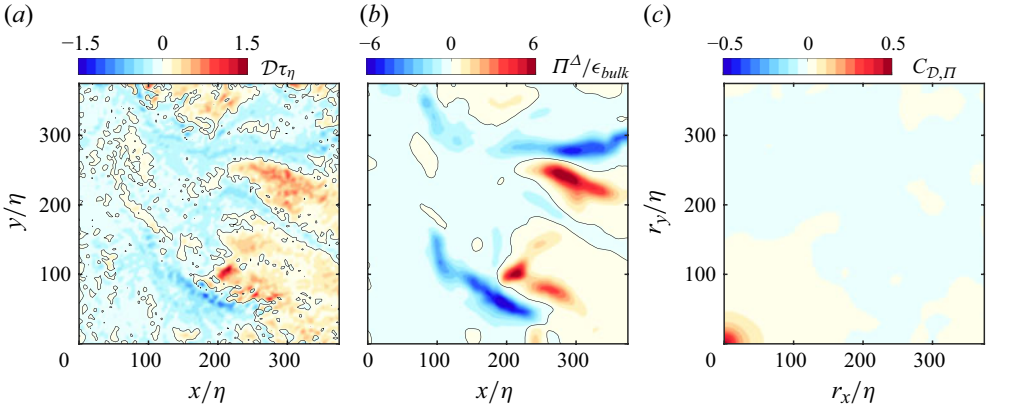


Figure 6. Instantaneous snapshots of (*a*) the divergence field and (*b*) the energy-flux field (filtering kernel size $\Delta = 30\eta$), and (*c*) the 2-D map of normalised correlation $C_{\mathcal{D},\Pi}$ in the 2-D plane 2 mm away from the free surface.

in physical space, based on the filter velocity field with kernel width Δ (see, among others, Pan & Banerjee 1995; Xiao *et al.* 2009; Lovecchio *et al.* 2015; Yao *et al.* 2024*a*; Zhu, Xie & Xia 2024). The energy flux at scale Δ is $\Pi^\Delta = \tau_{ij}^\Delta s_{ij}^\Delta$, where $\tau_{ij}^\Delta = (u_i u_j)^\Delta - u_i^\Delta u_j^\Delta$ and $s_{ij}^\Delta = (\partial_{x_j} u_i^\Delta + \partial_{x_i} u_j^\Delta)/2$ are the stress tensor and rate of strain, respectively. As an illustration, figures 6(*a*,*b*) show instantaneous snapshots of divergence field $\mathcal{D}$ and energy transfer flux field Π^Δ, respectively, for $\Delta = 30\eta$. These fields bear strong resemblance, with upscale energy fluxes collocated with regions of positive divergence, and vice versa. This can be quantified by the normalised correlation $C_{\mathcal{D},\Pi}$ in terms of their inner product (Savelsberg & van de Walter 2008):

$$C_{\mathcal{D},\Pi}(\boldsymbol{r}) = \frac{\overline{\mathcal{D}(\boldsymbol{x}+\boldsymbol{r},t)\cdot\Pi^\Delta(\boldsymbol{x},t)}}{\overline{\mathcal{D}\cdot\mathcal{D}}^{1/2}\,\overline{\Pi^\Delta\cdot\Pi^\Delta}^{1/2}}. \tag{3.1}$$

A significant correlation between $\mathcal{D}$ and Π^Δ can be seen in figure 6(*c*), with a maximum $C_{\mathcal{D},\Pi}(0) \approx 0.5$. Much weaker correlation between these quantities is found in the bulk, as shown in Appendix B. Analogous conclusions are drawn for different filter scales. This

https://doi.org/10.1017/jfm.2025.11071 Published online by Cambridge University Press

indicates that at the free surface, the local inter-scale energy transfer is correlated to the divergent flow structures along the free surface.

We close this section with a note on the applicability of the inter-scale energy transfer analysis to free-surface turbulent flows. While the surface flow energy is exchanged with the bulk turbulence beneath and therefore not conserved, this does not undermine the usefulness of the tools that we have adopted. In fact, this approach has been used extensively to uncover the dynamics of a wide array of flows (or portions of them) that exchange energy with adjacent part of the domain, describing pathways of energy transfer across scales, which is useful to both interpreting and modelling them.

In particular, the motion of the ocean free surface has been extensively investigated to determine whether its energy is passed prevalently to larger or smaller scales. For example, Balwada *et al.* (2022) analysed field data from surface drifters in the Gulf of Mexico and found evidence of a dual cascade, with far-reaching consequences for the modelling of oceanic turbulence. Likewise, Tedesco *et al.* (2024) used numerical simulations of the near-surface sub-mesoscale turbulence in the Drake Passage to show that eddies and fronts can cause an inverse cascade that replenishes the kinetic energy of mesoscale eddies. Beside surface flows, the dual nature of the cascade has been highlighted in many archetypical configurations, by restricting the analysis to portions of the domain that naturally exchange energy with the surroundings. For example, in wall-bounded turbulence, an inverse cascade was shown to exist at the buffer layer, transferring energy to larger spanwise scales at constant distance from the wall (Jiménez 1999; Cimarelli *et al.* 2016). In rotating Rayleigh–Bénard convection in the geostrophic regime, the spectral transfer term displays energy fluxes from smaller to larger scales when evaluated in the domain excluding the boundary layers, and such an inverse cascade is associated with the formation of a large barotropic vortex (Kunnen *et al.* 2016). By following a strategy similar to that in the present work, those studies revealed important aspects of the whole system dynamics, focusing on specific parts of the entire domain in which energy is not conserved but significant inter-scale energy transfers occur.

4. Conclusion

We have probed experimentally the cascade of energy associated with the free-surface flow above homogeneous turbulence, with negligible mean velocity, shear and waves. The free-surface boundary condition results in profoundly different dynamics compared to both 3-D and 2-D incompressible turbulence. Because energy and enstrophy are not conserved along the surface, classic arguments for the direction and magnitude of the inter-scale transfers cannot be used. We have therefore investigated the intensity, relative prevalence and mechanism behind the local (in space and time) inter-scale energy fluxes to smaller and larger scales. The direct evaluation of the inter-scale energy fluxes indicates that the direction of the cascade within the surface flow depends on its divergence: expansive and compressive states are responsible for energy passing to larger and smaller scales, respectively. Such fluxes in scale space are associated with upwelling and downwelling motions, respectively, and are much more intense than the characteristic ones in the bulk, where the nonlinear inter-scale transfer is in equilibrium with dissipation. Because the upwelling/expansive and downwelling/compressive states are approximately in balance, on average there is no sizeable net energy cascade in the present configuration.

These findings have far-reaching ramifications in the predictive understanding and modelling of this class of flows. In particular, since approximately half of the instantaneous inter-scale transfers of the surface flow energy are inverse, it is imperative for coarse-graining strategies such as large-eddy simulations to account for its backscatter by the

https://doi.org/10.1017/jfm.2025.11071 Published online by Cambridge University Press

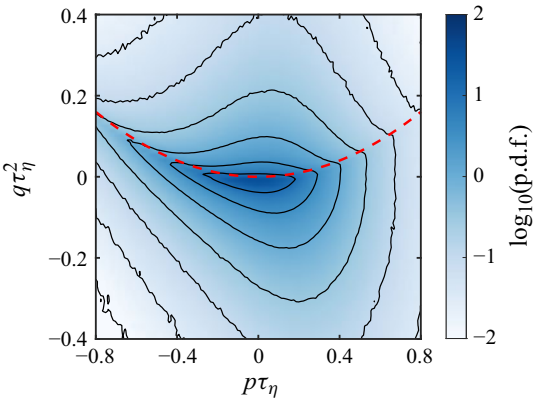


Figure 7. The joint p.d.f. of normalised p and q at $Re_\lambda = 326$ along the 2-D PIV plane in the centre of the water tank. The logarithmic contours range from 10^{-2} to 10^{1}, with adjacent contours being separated by half a decade, and the red dashed lines mark $q = p^2/4$.

sub-grid scales. We note that while the average net energy transfer is negligibly small, the instantaneous/local fluxes in both directions are much larger than the direct transfer rate in the bulk. Therefore, modelling approaches aiming to resolve the spatio-temporal dynamics need to capture the transfers in both directions. An example of the importance of such mechanisms is offered by the recent numerical study of surface geostrophic turbulence in the upper ocean by Xiong *et al.* (2025). While their system is distinct from ours due to the role of rotation and buoyancy fluctuations, it also exhibits strikingly similar dynamics associated to the divergence of the surface flow: the compression of cold cyclones by the large-scale background flow sustains downscale energy transfers, while the expansion of warm filaments drives energy upscale. Importantly, the direction of the energy cascade is related to the relative rates of dispersion forwards and backwards in time, which have implications for estimating contaminant spread and concentration fluctuations (Bragg, Ireland & Collins 2016).

The present work raises numerous further questions. What is the characteristic spatial and temporal extent of the upwelling/expansion and downwelling/compression events? What sets the magnitude of the inter-scale fluxes associated with them? How are these dynamics affected by surface deformation and surfactants? Further studies in these directions are underway.

Acknowledgements. We thank H. Yao and H. Zhu for inspiring discussions and suggestions.

Funding. Y.L. gratefully acknowledges funding from the National Natural Science Foundation of China (NSFC grant no. 12572295), the Opening fund of State Key Laboratory of Nonlinear Mechanics, and the Opening fund of State Key Laboratory for Strength and Vibration of Mechanical Structures (no. SV2023-KF-03). F.C. gratefully acknowledges funding from the Swiss National Science Foundation (project no. 200021-207318).

Declaration of interests. The authors report no conflict of interest.

Appendix A. Joint p.d.f of p and q of the 3-D homogeneous turbulence in the bulk

Figure 7 presents the joint p.d.f. of the normalised quantities p and q at $Re_\lambda = 326$, measured from a 2-D section of the homogeneous turbulence in the bulk flow region. When compared to the results measured 2 mm away from the free surface (as shown in figure 2*a*4), the probability distribution of p exhibits notably lighter tails, suggesting a

https://doi.org/10.1017/jfm.2025.11071 Published online by Cambridge University Press

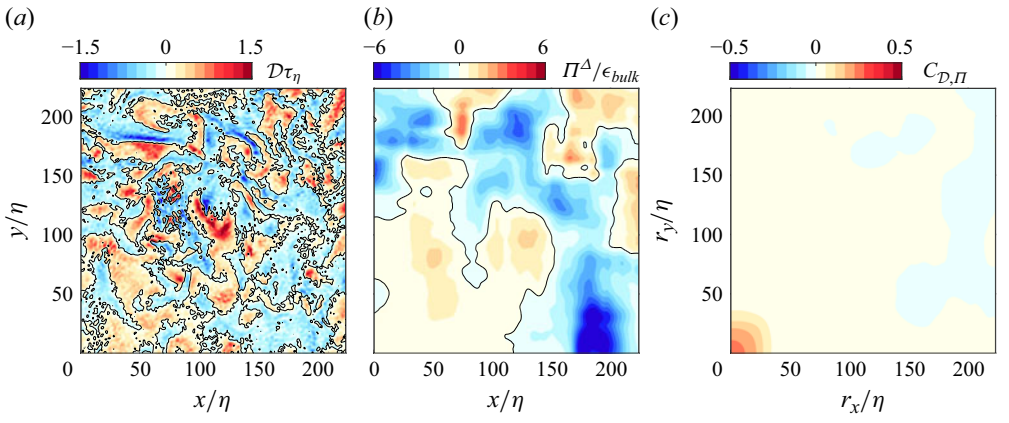


Figure 8. Instantaneous snapshots of (*a*) the divergence field and (*b*) the energy flux field (filtering kernel size $\Delta = 30\eta$), and (*c*) the 2-D map of normalised correlation $C_{\mathcal{D},\Pi}$ in the 2-D plane in the bulk far away from the free surface.

significant reduction in the occurrence of intensive expanding and contracting patterns in the bulk of turbulence.

Appendix B. Inter-scale energy transfer of the 3-D homogeneous turbulence in the bulk

Figures 8(*a*,*b*) show instantaneous snapshots of the divergence field $\mathcal{D}$ and energy transfer flux field Π^Δ with $\Delta = 30\eta$ along the 2-D PIV plane in the bulk, respectively. The resemblance between the divergence field and the energy flux field is notably less significant than that along the free surface, which can be also seen in the correlation relation in figure 8(*c*), i.e. the maximum correlation $\mathcal{C}_{\mathcal{D},\Pi}(0) \approx 0.2$.

References

Alexakis, A. & Biferale, L. 2018 Cascades and transitions in turbulent flows. *Phys. Rep.* **767–769**, 1–101.

Balwada, D., Xie, J.H., Marino, R. & Feraco, F. 2022 Direct observational evidence of an oceanic dual kinetic energy cascade and its seasonality. *Sci. Adv.* **8**, eabq2566.

Boffetta, G., Davoudi, J., Eckhardt, B. & Schumacher, J. 2004 Lagrangian tracers on a surface flow: the role of time correlations. *Phys. Rev. Lett.* **93**, 134501.

Boffetta, G., Musacchio, S., Mazzino, A. & Rosti, M.E. 2023 Transient inverse energy cascade in free surface turbulence. *Phys. Rev. Fluids* **8**, 034601.

Bragg, A.D., Ireland, P.J. & Collins, L.R. 2016 Forward and backward in time dispersion of fluid and inertial particles in isotropic turbulence. *Phys. Fluids* **28** (1), 013305.

Brocchini, M. & Peregrine, D.H. 2001 The dynamics of strong turbulence at free surfaces. Part 1. Description. *J. Fluid Mech.* **449**, 225–254.

Brumley, B.H. & Jirka, G.H. 1987 On the normalized turbulent energy dissipation rate. *J. Fluid Mech.* **183**, 235–263.

Cardesa, J.I., Mistry, D., Gan, L. & Dawson, J.R. 2013 Invariants of the reduced velocity gradient tensor in turbulent flows. *J. Fluid Mech.* **716**, 597–615.

Carter, D., Petersen, A., Amili, O. & Coletti, F. 2016 Generating and controlling homogeneous air turbulence using random jet arrays. *Exp. Fluids* **57**, 1–15.

Carter, D.W. & Coletti, F. 2017 Scale-to-scale anisotropy in homogeneous turbulence. *J. Fluid Mech.* **827**, 250–284.

Carter, D.W. & Coletti, F. 2018 Small-scale structure and energy transfer in homogeneous turbulence. *J. Fluid Mech.* **854**, 505–543.

Cimarelli, A., Boga, G., Pavan, A., Costa, P. & Stalio, E. 2024 Spatially evolving cascades in wall turbulence with and without interface. *J. Fluid Mech.* **987**, A4.

https://doi.org/10.1017/jfm.2025.11071 Published online by Cambridge University Press

CIMARELLI, A., DE ANGELIS, E. & CASCIOLA, C.M. 2013 Paths of energy in turbulent channel flows. *J. Fluid Mech.* **715**, 436–451.
CIMARELLI, A., DE ANGELIS, E., JIMÉNEZ, J. & CASCIOLA, C.M. 2016 Cascades and wall-normal fluxes in turbulent channel flows. *J. Fluid Mech.* **796**, 417–436.
CIMARELLI, A., MOLLICONE, J.P., VAN REEUWIJK, M. & DE ANGELIS, E. 2021 Spatially evolving cascades in temporal planar jets. *J. Fluid Mech.* **910**, A19.
CRESSMAN, J.R., DAVOUDI, J., GOLDBURG, W.I. & SCHUMACHER, J. 2004 Eulerian and Lagrangian studies in surface flow turbulence. *New J. Phys.* **6**, 53.
CSANADY, G.T. 1963 Turbulent diffusion in Lake Huron. *J. Fluid Mech.* **17**, 360–384.
DEIKE, L. 2022 Mass transfer at the ocean–atmosphere interface: the role of wave breaking, droplets, and bubbles. *Annu. Rev. Fluid Mech.* **54**, 191–224.
ECKHARDT, B. & SCHUMACHER, J. 2001 Turbulence and passive scalar transport in a free-slip surface. *Phys. Rev. E* **64**, 016314.
VAN EMMERIK, T. & SCHWARZ, A. 2020 Plastic debris in rivers. *WIREs Water* **7**, e1398.
GOLDBURG, W.I., CRESSMAN, J.R., VÖRÖS, Z., ECKHARDT, B. & SCHUMACHER, J. 2001 Turbulence in a free surface. *Phys. Rev. E* **63**, 065303.
GOMES-FERNANDES, R., GANAPATHISUBRAMANI, B. & VASSILICOS, J.C. 2015 The energy cascade in near-field non-homogeneous non-isotropic turbulence. *J. Fluid Mech.* **771**, 676–705.
GUO, X. & SHEN, L. 2010 Interaction of a deformable free surface with statistically steady homogeneous turbulence. *J. Fluid Mech.* **658**, 33–62.
HERLINA, H. & WISSINK, J.G. 2014 Direct numerical simulation of turbulent scalar transport across a flat surface. *J. Fluid Mech.* **744**, 217–249.
HERLINA, N. & JIRKA, G.H. 2008 Experiments on gas transfer at the air–water interface induced by oscillating grid turbulence. *J. Fluid Mech.* **594**, 183–208.
HILL, R.J. 2002 Exact second-order structure–function relationships. *J. Fluid Mech.* **468**, 317–326.
HUNT, J.C.R. & GRAHAM, J.M.R. 1978 Free-stream turbulence near plane boundaries. *J. Fluid Mech.* **84**, 209–235.
JÄHNE, B. & HAUSSECKER, H. 1998 Air–water gas exchange. *Annu. Rev. Fluid Mech.* **30**, 443–468.
JIMÉNEZ, J. 1999 The physics of wall turbulence. *Phys. A: Stat. Mech. Appl.* **263**, 252–261.
KOLMOGOROV, A.N. 1941 The local structure of turbulence in incompressible viscous fluid for very large Reynolds numbers. *Dokl. Akad. Nauk SSSR* **30**, 301.
KUMAR, S., GUPTA, R. & BANERJEE, S. 1998 An experimental investigation of the characteristics of free-surface turbulence in channel flow. *Phys. Fluids* **10**, 437–456.
KUNNEN, R.P., OSTILLA-MÓNICO, R., VAN DER POEL, E.P., VERZICCO, R. & LOHSE, D. 2016 Transition to geostrophic convection: the role of the boundary conditions. *J. Fluid Mech.* **799**, 413–432.
LAMRIBEN, C., CORTET, P.-P. & MOISY, F. 2011 Direct measurements of anisotropic energy transfers in a rotating turbulence experiment. *Phys. Rev. Lett.* **107**, 024503.
LI, Y., SANNESS SALMON, H., HASSAINI, R.,CHANG, K.,MUCIGNAT, C. & COLETTI, F. 2025 Spatiotemporal scales of motion and particle clustering in free-surface turbulence. *Phys. Rev. Fluids* **10**, 034602.
LI, Y., WANG, Y., QI, Y. & COLETTI, F. 2024 Relative dispersion in free-surface turbulence. *J. Fluid Mech.* **993**, R2.
LOVECCHIO, S., MARCHIOLI, C. & SOLDATI, A.2013 Time persistence of floating-particle clusters in free-surface turbulence. *Phys. Rev. E* **88**, 033003.
LOVECCHIO, S., ZONTA, F. & SOLDATI, A. 2015 Upscale energy transfer and flow topology in free-surface turbulence. *Phys. Rev. E* **91**, 033010.
MAGNAUDET, J. 2003 High-Reynolds-number turbulence in a shear-free boundary layer: revisiting the Hunt–Graham theory. *J. Fluid Mech.* **484**, 167–196.
MARATI, N., CASCIOLA, C.M. & PIVA, R. 2004 Energy cascade and spatial fluxes in wall turbulence. *J. Fluid Mech.* **521**, 191–215.
MCKENNA, S.P. & MCGILLIS, W.R. 2004 The role of free-surface turbulence and surfactants in air–water gas transfer. *Intl J. Heat Mass Transfer* **47**, 539–553.
MOISY, F. & JIMÉNEZ, J. 2004 Geometry and clustering of intense structures in isotropic turbulence. *J. Fluid Mech.* **513**, 111–133.
PAN, Y. & BANERJEE, S. 1995 A numerical study of free-surface turbulence in channel flow. *Phys. Fluids* **7**, 1649–1664.
PERRY, A.E. & CHONG, M.S. 1994 Topology of flow patterns in vortex motions and turbulence. *Appl. Sci. Res.* **53** (3), 357–374.

https://doi.org/10.1017/jfm.2025.11071 Published online by Cambridge University Press

PORTELA, F.A., PAPADAKIS, G. & VASSILICOS, J.C. 2017 The turbulence cascade in the near wake of a square prism. *J. Fluid Mech.* **825**, 315–352.

QI, Y., LI, Y. & COLETTI, F. 2025*a* Small-scale dynamics and structure of free-surface turbulence. *J. Fluid Mech.* **1007**, A3.

QI, Y., XU, Z. & COLETTI, F. 2025*b* Restricted Euler dynamics in free-surface turbulence. *J. Fluid Mech.* **1002**, A38.

RUTH, D.J. & COLETTI, F. 2024 Structure and energy transfer in homogeneous turbulence below a free surface. *J. Fluid Mech.* **1001**, A46.

SANNESS SALMON, H., BAKER, L.J., KOZAREK, J.L. & COLETTI, F. 2023 Effect of shape and size on the transport of floating particles on the free surface in a natural stream. *Water Resour. Res.* **59** (10), e2023WR035716.

SAVELSBERG, R. & VAN DE WALTER, W. 2008 Turbulence of a free surface. *Phys. Rev. Lett.* **100**, 034501.

SCHUMACHER, J. & ECKHARDT, B. 2002 Clustering dynamics of Lagrangian tracers in free-surface flows. *Phys. Rev. E* **66**, 017303.

VAN SEBILLE, E., *et al.* 2020 The physical oceanography of the transport of floating marine debris. *Environ. Res. Lett.* **15**, 023003.

SHEN, L., ZHANG, X., YUE, D.K. & TRIANTAFYLLOU, G.S. 1999 The surface layer for free-surface turbulent flows. *J. Fluid Mech.* **386**, 167–212.

SMELTZER, B.K., RØMCKE, O., HEARST, R.J. & ELLINGSEN, S.Å. 2023 Experimental study of the mutual interactions between waves and tailored turbulence. *J. Fluid Mech.* **962**, R1.

TEDESCO, P.F., BAKER, L.E., NAVEIRA GARABATO, A.C., MAZLOFF, M.R., GILLE, S.T., CAULFIELD, C.P. & MASHAYEK, A. 2024 Spatiotemporal characteristics of the near-surface turbulent cascade at the submesoscale in the Drake Passage. *J. Phys. Oceanogr.* **54**, 187–215.

VALENTE, P.C. & VASSILICOS, J.C. 2015 The energy cascade in grid-generated non-equilibrium decaying turbulence. *Phys. Fluids* **27** (4), 045103.

VARIANO, E.A. & COWEN, E.A. 2008 A random-jet-stirred turbulence tank. *J. Fluid Mech.* **604**, 1–32.

VARIANO, E.A. & COWEN, E.A. 2013 Turbulent transport of a high-Schmidt-number scalar near an air–water interface. *J. Fluid Mech.* **731**, 259–287.

VASSILICOS, J.C. 2015 Dissipation in turbulent flows. *Annu. Rev. Fluid Mech.* **47**, 95–114.

XIAO, Z., WAN, M., CHEN, S. & EYINK, G.L. 2009 Physical mechanism of the inverse energy cascade of two-dimensional turbulence: a numerical investigation. *J. Fluid Mech.* **619**, 1.

XIONG, Y., ZHANG, Y., LI, X. & XIE, L. 2025 Divergence-driven upscale energy transfer in the high-order surface geostrophic turbulence. *Phys. Rev. Fluids* **10** (8), 084604.

YAO, H., SCHNAUBELT, M., SZALAY, A.S., ZAKI, T.A. & MENEVEAU, C. 2024*a* Comparing local energy cascade rates in isotropic turbulence using structure–function and filtering formulations. *J. Fluid Mech.* **980**, A42.

YAO, H., YEUNG, P.K., ZAKI, T.A. & MENEVEAU, C. 2024*b* Forward and inverse energy cascade in fluid turbulence adhere to Kolmogorov's refined similarity hypothesis. *Phys. Rev. Lett.* **132** (16), 164001.

YASUDA, T. & VASSILICOS, J.C. 2018 Spatio-temporal intermittency of the turbulent energy cascade. *J. Fluid Mech.* **853**, 235–252.

ZHU, H., XIE, J. & XIA, K. 2024 Flow patterns and energy spectra in forced quasi-two-dimensional turbulence: effect of system size and damping rate. *J. Fluid Mech.* **996**, A39.

https://doi.org/10.1017/jfm.2025.11071 Published online by Cambridge University Press